Chlorobaculum tepidum Outer Membrane Vesicles May Transport Biogenic Elemental Sulfur.

Vadesse L. Noundou[1,2], Amalie Levy[2,4†], Shannon Modla[2], Yanbao Yu[5], Jing Qu[6], Thomas E. Hanson[1,2,3*]

[1] Department of Biological Sciences, University of Delaware, Newark, DE, 19716, USA
[2] Delaware Biotechnology Institute, Newark, DE, 19713, USA
[3] School of Marine Science and Policy, University of Delaware, Newark, DE, 19716, USA
[4] Department of Chemical and Biomolecular Engineering, University of Delaware, Newark, DE, 19716, USA
[5] Department of Chemistry & Biochemistry, University of Delaware, Newark, DE, 19716, USA
[6] Advanced Materials Characterization Laboratory, University of Delaware, Newark, DE, 19716, USA

[*]Corresponding author:
Thomas E. Hanson, E-mail: tehanson@udel.edu, Tel: (302) 831-3404

†Current affiliation:
Janssen Research & Development, LLC, Malvern, PA 19355

Keywords: Chlorobiaceae, *Chlorobaculum tepidum*, sulfur globules, outer membrane vesicles, proteomics, Raman spectroscopy, NanoIR spectroscopy

ABSTRACT

Outer membrane-derived vesicles (OMVs) have been studied in different phyla of Gram-negative bacteria, most extensively in the Pseudomonadota, where they have been shown to participate in diverse biological and environmental processes. To date, the production of OMVs has not been reported in the Chlorobiaceae within the phylum Chlorobiota. *Chlorobaculum. tepidum* is the model organism for the Chlorobiaceae that synthesizes and consumes insoluble extracellular sulfur (S(0)) globules by an unknown mechanism. Here, we report evidence implicating outer membrane vesicles in biogenic S(0) globule synthesis. We demonstrate that *Cba. tepidum* secretes OMVs in the extracellular milieu, and that OMV concentration and size vary with growth conditions, particularly sulfide concentration. A core of 31 proteins involved in diverse biological processes such as cell wall biogenesis, inorganic ion transport and metabolism were found to be shared between OMVs, extracellular S(0) globules and *Cba. tepidum* intact cells. Multiple analytical methods indicated that OMVs contain S(0) and that OMVs and biogenic S(0) globules share protein and polysaccharide signatures, including lipooligosaccharides. Together these lines of evidence indicate that *Cba. tepidum*'s OMVs are one component of sulfur transport between cells and extracellular sulfur globules.

IMPORTANCE

All living cells must exchange material with their environment while maintaining cellular integrity. This is a particular challenge for materials that are not water soluble, yet many bacteria utilize insoluble materials for energy conservation and as nutrients for growth. Here we show that *Cba. tepidum* makes outer membrane vesicles and that these vesicles are likely involved in the exchange of material with extracellular elemental sulfur globules formed and consumed by *Cba. tepidum* as part of its energy metabolism based on oxidizing reduced sulfur compounds like hydrogen sulfide. These data expand our basic understanding of *Cba. tepidum*'s metabolism. As elemental sulfur is an industrial by-product with a limited number of uses, the information here may help enable the use of additional sulfur compounds by *Cba. tepidum* to drive the synthesis of biomass and/or specialty biochemicals from waste elemental sulfur by this autotrophic bacterium.

INTRODUCTION

Many microbes interact with solids as part of their energy metabolism or to obtain elements required for growth. In either case, insoluble materials must pass through the cell envelope while maintaining cellular envelope integrity. Microbe-mineral interactions often occur in the context of redox reactions for energy metabolism. Examples include the production of extracellular sulfur globules (S(0)) by sulfide oxidation and their further oxidation to sulfate by phototrophic bacteria (1) or the utilization of Fe- and Mn-oxides as terminal electron acceptors (2, 3). These microbe-mineral interactions drive many biogeochemical cycles and the bioremediation of organic and inorganic pollutants (4). In Gram-negative bacteria, outer membrane vesicles (OMVs) are one mechanism used to interact with surfaces for multiple functional outcomes (5). For example, *Acinetobacter baumannii* OMVs enriched in TonB-dependent transporters enabled the acquisition of insoluble nutrients such as iron (6). Recently, OMVs containing a truncated form of lipopolysaccharide (LPS) were implicated as a key mechanism of *Geobacter sulfurreducens*' elimination of uranium particles (7). Although OMVs have been intensively studied in heterotrophic Pseudomonadota, less is known about the production, composition, and physiological role of OMVs outside of this phylum.

OMVs are small (20-300 nm) spherical structures produced by Gram-negative bacteria via OM vesiculation (21). OMVs contain phospholipids, LPS or lipooligosaccharides (LOS), and outer membrane proteins (OMPs). OMVs also contain cargo that may include nucleic acids (DNA and RNA), periplasmic components, housekeeping proteins, and enzymes (22–24). OMVs were once regarded as cell debris or microscopy artifacts. Nowadays, OMVs have been shown to participate in diverse biological processes, such as transferring and delivering their components to the extracellular environment (25) and host-microbe interactions (26).

Chlorobaculum tepidum (Cba. tepidum) is an anaerobic photoautotrophic Gram-negative bacterium, but little is known about the composition and metabolism of the outer membrane

(OM) in this organism or the Chlorobiaceae more broadly. *Cba. tepidum* is a model organism of the Green Sulfur Bacteria (GSB) due to rapid growth in culture (8), a sequenced and annotated genome (9), and genetic tools (10–12). *Cba. tepidum* utilizes a variety of inorganic sulfur compounds as electron donors to fix CO_2 through the reverse TCA cycle (13, 14). *Cba. tepidum* both forms and consumes extracellular S(0) globules, but the details of how this occurs are unclear (1). However, the enzymes catalyzing S(0) production and consumption are believed to reside in the periplasm between the OM and cell membrane (15, 16). As S(0) is extracellular, there must be a transport mechanism for S(0) to cross the outer membrane during its production and consumption. Time-lapse microscopy of *Cba. tepidum* documents S(0) globules appearing in cultures with no visible connection to cells and increasing in size during growth on sulfide. S(0) globules produced by the wild type *Cba. tepidum* strain are roughly spherical and 1-2 μm in diameter (17, 20), while those produced by a mutant strain that cannot oxidize S(0) are larger, up to ~8 μm in diameter (1). *Cba. tepidum* cells are typically ~0.5 μm wide by 1-2 μm long (1, 17, 20).

Cba. tepidum grows well with elemental sulfur that it has synthesized, i.e. biogenic S(0) globules, as a sole electron donor and a sub-population of cells is tighly attached to S(0) during its utilization (1). *Cba. tepidum* S(0) globules have a proteome (1, 19) that includes proteins CT1320.1 and CT1305, OM proteins only found in the Chlorobiaceae and *Geobacter* spp., which also rely on interactions with insoluble minerals for energy metabolism (18). Biogenic S(0) globule utilization cannot be catalyzed by small metabolites or secreted soluble proteins as separating *Cba. tepidum* cells from biogenic S(0) with dialysis membranes ranging from 50 to 100 kDa prevented growth. Thus, relatively large proteins or complexes are required for biogenic S(0) utilization (1). Separately, time-lapse phase contrast microscopy showed that while some cells directly contact biogenic S(0), individual S(0) globules can be formed and consumed in cultures without direct contact by cells (17). Growth rates of cells that were not attached to S(0) globules were the same as those attached to S(0). Thus, material is released that allows cells at a distance from S(0) globules to grow as well as those that are attached. Spectroscopic characterization of *Cba. tepidum* S(0) globules indicated the presence of proteins and polysaccharides as an organic coating that was proposed to slow the conversion of amorphous biogenic S(0) to crystalline sulfur (20). *Cba. tepidum* biogenic S(0) globules stained with the membrane specific dye FM 1-43FX (20), suggesting that they contain lipids. Collectively, these observations from prior experiments suggest that *Cba. tepidum* S(0) globule formation and consumption involves components that contain outer membrane proteins, polysaccharides, lipids, in complexes larger than 100 kDa, but smaller than the resolution limits of phase-contrast microscopy. OMVs are a good candidate for these components.

Microbial production of extracellular S(0) associated with organic materials is well known, but mechanistic details underlying its formation are scarce (1, 17, 20, 27–29). S(0) transport by cytoplasmic membrane vesicles has been observed in Archaea, e.g. Gorlas *et al.* (30) reported

that *Thermococcus* species produced vesicles containing S(0) solely when S(0) was added to the growth medium. They hypothesized this was to remove excess S(0) not used for growth, preventing the accumulation of toxic levels in the cytoplasm. Alternatively, the formation of organic associated amorphous S(0) has been proposed to be a precipitation process during sulfide oxidation in the presence of organics that can occur in spent medium in the absence of cells; a process called organomineralization (27, 28, 31, 32).

We hypothesize that *Cba. tepidum* produces OMVs that participate in S(0) transport between cells and extracellular S(0) globules. If the hypothesis is correct, then we predict proteomic analysis of OMV cargo should detect previously identified S(0) globule proteins (CT1305 and CT1320.1) and that there should be substantial overlap between OMV and S(0) globule proteomes. We would also expect lipid A in the form of lipopolysaccharide (LPS) or lipooligosaccharide (LOS) should be present in both OMVs and S(0) globules. Finally, we would also expect that OMV abundance will be higher when S(0) is actively being produced or consumed by *Cba. tepidum*. Here, we test these predictions through a combination of OMV purification, proteomic and LPS analysis of both OMVs and S(0) globules, and OMV quantification under different growth conditions. Raman spectroscopy was used to investigate the chemical signatures of OMVs and S(0). The data are consistent with a model where OMVs participate in extracellular S(0) globule formation characteristic of the Chlorobiota. Furthermore, the results reported here provide significant new information on OM structure and function outside the Pseudomonadota. In the following sections, we use the term 'particle' to describe materials that were analyzed to determine if they were OMVs or not. We only use the term OMV after presenting data that their size and molecular composition of *Cba. tepidum* extracellular particles is consistent with them indeed being OMVs.

RESULTS AND DISCUSSION

Cba. tepidum secretes extracellular particles during growth.

While OMV secretion is considered a universal process among Gram-negative bacterial species (33, 34), most observations to date are from heterotrophic members of the phylum Pseudomonadota, formerly Proteobacteria (35–37). *Cba. tepidum* is a member of the phylum Chlorobiota, which is sister to the phylum Bacteroidota and distantly related to the Pseudomonadota. Therefore, we examined *Cba. tepidum* cultures for extracellular particles by microfluidic resistive pulse sensing (MRPS) analysis of 0.2 μm culture filtrates after 8 h (lag phase), 14 h (early-exponential phase), and 24 h (late-exponential phase) of growth. Briefly, MRPS detects and measures particles based on changes in electrical resistance as particles pass through a microfluidic pore that is charged held at a set voltage. The size range of particles detectable in these experiments was from ~40 nm to 400 nm. The number of particles detected was highest during the early-exponential growth phase (14 h of growth, Fig. 1A) and these particles contained protein (Fig. 1B). Protein and particle concentrations displayed the same pattern across growth phases. We chose early-exponential phase samples to produce large

160 amounts of particles for more detailed analysis because of the larger particle concentration and to
161 minimize capturing debris deriving from cell death or nutrient limitation during later growth
162 stages (41–43). Direct observation of *Cba. tepidum* cells in 14 h culture samples by TEM found
163 vesicles at the outer membrane (Fig. 2A, B) suggesting that *Cba. tepidum* actively produces
164 particles via OM blebbing. Particles purified from the early-exponential imaged by negative stain
165 TEM were spherical and displayed a cavity surrounded by a stained membrane (Fig. 2C, D).
166 These data demonstrate particle production by *Cba. tepidum* shares similarities with OMV
167 production: growth phase-dependence, particles appear to be produced by OM blebbing, and
168 TEM images resembling a deflated ball.

169 **Particles produced by *Cba. tepidum* are the same size as OMVs and contain**
170 **lipooligosaccharides.**

171 *Cba. tepidum* can grow on sulfide, thiosulfate, or biogenic S(0) as electron donors. Therefore, we
172 examined whether particles differed when they were purified (Fig. S1) from cultures grown on
173 single electron donors or the combination of sulfide and thiosulfate in Pf-7, the standard growth
174 condition (1, 8). *Cba. tepidum* growth rate was not significantly different between the growth
175 conditions (data not shown). Particles were characterized both by transmission electron
176 microscopy (TEM) and MRPS. TEM imaging requires sample concentration by
177 ultracentrifugation and chemical treatment prior to imaging, while MRPS provides information
178 on particle size and concentration after 0.2 µm filtration of the supernatant as the sole sample
179 preparation step (Fig. S1B). Therefore, we utilized MRPS to compare the concentration and size
180 of particles across growth conditions, while TEM image analysis was used to check particle
181 morphology and size. Mature S(0) globules produced by *Cba. tepidum* are larger than 0.2 µm
182 and should not be present in these samples (1, 17). The particle size distributions by TEM (10-
183 105 nm) and MRPS (40-125 nm) overlapped (Fig. S2), with the difference likely being the size
184 limit of detection for the MRPS cartridge being ~40 nm. Particles produced when thiosulfate was
185 the sole electron donor were slightly larger by MRPS than particles released under other
186 conditions, but the size distribution of *Cba. tepidum* particles purified from all conditions
187 overlapped and is consistent with published values for OMVs (Fig. 3A). Regardless of the
188 electron donor, the counted particles contained protein, with a linear relationship between
189 particle and protein concentrations (Fig. 3B), suggesting that particles have a constant
190 concentration of protein per unit of particle volume
191
192 Lipopolysaccharide (LPS), the major component of the outer leaflet of the OM, plays a crucial
193 role in the stability and permeability of the OM and should be present in *Cba. tepidum* particles
194 if they are OMVs. Therefore, we tested whether particles and biogenic S(0) produced by *Cba.*
195 *tepidum* contain LPS. The *Cba. tepidum* genome does contain genes for lipid A biosynthesis
196 (data not shown), but the structure of the outer membrane lipids has not been established to our
197 knowledge. Tricine SDS-PAGE was used to visualize material produced by an LPS purification
198 protocol: material from *Cba. tepidum* whole cells or purified particles (Fig. S1A) resolved in a
199 single low molecular weight band (Fig. 3C) while material purified from biogenic S(0) resolved

200 into two bands (Fig. 3D), with the lower molecular weight band migrating identically to that
201 from cells and particles. The *E. coli* purified LPS standard produced a laddered pattern
202 characteristic of an O antigen (Fig. 3C). Therefore, we conclude that *Cba. tepidum* makes
203 lipooligosaccharide (LOS), composed of lipid A and an inner core oligosaccharide (band 1).
204 *Bacteroides thetaiotamicron,* a member of the phylum Bacteroidota more closely related to *Cba.*
205 *tepidum* than *E. coli*, also synthesizes LOS (44). Similarly, Meißner *et al.* (45) showed that
206 purified OM lipid from *Chlorobium vibrioforme* had no O antigen repeating units, i.e. it is LOS.
207 The identity of band 2 observed in biogenic S(0) is unclear, but the staining method used is
208 specific for sugars, e.g. glycolipids like those in LPS and LOS. These samples did not contain
209 any material that stained with SYPRO Ruby (data not shown), indicating that the LPS
210 preparations were protein-free.
211
212 The identity of the material in the LPS preparations was further established by mass
213 spectrometry and an HPLC assay for the inner core sugar 2-ketodeoxy-octulosonic acid (KDO).
214 Masses consistent with lipid A were observed in electrospray ionization Fourier transform MS
215 after mild acid hydrolysis of LOS isolated from whole cells, OMVs, and biogenic S(0). Different
216 forms of lipid A were detected in each sample. The hepta-acyl form was found in WC, HS-OMV,
217 and S(0) (*m/z* 1851, 1894, 1925, 1926, 1912), while the penta-acyl form was found only in Pf7-
218 OMV (*m/z* 1659, 1705, 1795). The observed diversity of lipid A forms in *Cba. tepidum* suggests
219 some differences in their acyl chain length and number depending on growth condition, which
220 may in turn affect or be a result of OMV production (46–48). KDO was detected in all samples
221 tested, with the highest level found in whole cells (Fig. 2E). No KDO was detected in any mock
222 samples: PBS and chemical sulfur purchased from Sigma-Aldrich using the same reagents and
223 buffers for preparing the samples. Taken together with the data above on particle size, TEM
224 appearance, and protein content, the detection of glycolipid staining, Lipid A, and KDO in
225 particles produced by *Cba. tepidum* confirms that these are indeed OMVs and this term will be
226 used hereafter. Detection of these signatures in biogenic S(0) supports a hypothesis where OMVs
227 may be one route of transfer of S(0) to extracellular S(0) globules, which is consistent with prior
228 data on the composition of *Cba. tepidum* S(0) globules (1, 19, 20).
229
230 **Proteome analysis of *Cba. tepidum* OMVs versus whole cells and biogenic Sulfur**
231 Previously, we showed that *Cba. tepidum* S(0) globules contained the proteins CT1305 and
232 CT1320.1 (1), which are only shared with *Geobacter* spp. that also interact with insoluble phases
233 for energy metabolism. Deeper analysis of these extracts by shotgun proteomics indicated that
234 biogenic S(0) contained a significant proteome of at least 96 proteins (Supplemental Table S1),
235 which is lower than the 696 S(0)-associated proteins recently identified by Lyratzakis *et al.* (19).
236 Here, we generated new shotgun proteomic datasets for *Cba. tepidum* OMVs, biogenic S(0), and
237 whole cells of *Cba. tepidum* to control for S(0)-attached cells that are difficult to separate from
238 biogenic S(0) (1). The whole cell samples were diluted to an equal concentration of
239 bacteriochlorophyll (Bchl) *c* observed in biogenic S(0). This assumes that Bchl *c* in biogenic

240 S(0) is from adherent cells and was done to normalize the total amount of protein in the whole
241 cell samples to that of adhered cells in biogenic S(0). This is needed for label-free quantification
242 comparisons between samples. A total of 1,447 unique proteins were identified across all
243 samples (Fig. 4A), with 757 of these detected in S(0) globules, somewhat more than the number
244 observed by Lyratzakis *et al.* (19). OMVs from thiosulfate-only cultures only contained two
245 proteins, CT0068 and CT2144, which are both outer membrane beta-barrel proteins, suggesting
246 that electron donors might play a key role in shaping the cargo carried by OMVs. For example,
247 Liu *et al.* (49) showed that differences in redox potential might impact the packaging of specific
248 molecules (lipids, enzymes, proteins, toxins) into OMVs. Based on the limited proteome in
249 thiosulfate-OMVs, this condition was excluded from further comparative analysis.
250
251 OMV proteomes from cultures grown on sulfide (HS-OMVs), sulfide + thiosulfate (PF7-OMVs),
252 purified biogenic S(0) globules, and diluted whole-cells shared 31 proteins detected in at least
253 two independent samples for each group (Table 1), which we considered to be the OMV core
254 proteome. This is a more conservative estimate than the Venn diagram (Fig. 4A), which only
255 required detection of a protein in one of the three independent samples within a group. The
256 functional annotations of the 31 proteins include porin activity, electron transfer activity, and
257 trafficking of unfolded proteins. Furthermore, two periplasmic proteins, SurA (CT2264) and
258 DegP (CT1447), identified in the initial S(0) globule proteome (Supplemental Table S1), were
259 also found in HS-OMVs. Based on experimental evidence (50) and a computational model (51),
260 SurA is believed to be involved in the trafficking of unfolded outer membrane proteins, while
261 DegP has protease activity and is involved in the degradation of misfolded proteins, preventing
262 the accumulation of waste in the periplasm. CT1305, one of two poorly characterized proteins
263 shared with *Geobacter* spp. and detected in the initial S(0) proteome (Supplemental Table S1),
264 was detected in PF7-OMVs, S(0) globules, and whole cells, but not HS-OMVs, so it was not
265 included in the OMV core. The other, CT1320.1, was not detected in any of the samples.
266
267 We assessed the relationship between protein composition and sample characteristics using
268 Principal Components Analysis (PCA, Fig. 4B) of log2 transformed label-free quantification
269 abundance data. Our analysis showed that the first two components accounted for a high
270 proportion of the total variation (87.9%) between samples, with those of each group clustering
271 together. The OMV and S(0) samples were well separated from whole cells on the PC1 axis
272 (80.6% of variation). The OMV and S(0) samples also separated along the PC2 axis (7.3% of
273 variation), indicating that they are distinct from one another. Proteins were grouped by their
274 predicted subcellular localization and the cumulative loadings for these groups (Fig. 4B, blue
275 dashed arrows) indicate that cytoplasmic proteins are responsible for separation of the whole cell
276 samples from the others. The loadings for predicted outer membrane, periplasmic and
277 extracellular proteins are very similar and aligned along the PC2 axis, suggesting that they
278 strongly contribute to separation of samples in this dimension.
279

The effect of electron donors on OMV abundance.

The relationship between the proteomes of OMV and biogenic S(0) prompted us to examine whether sulfide concentration modulated OMV production. We hypothesized that increasing sulfide concentrations will cause *Cba. tepidum* to release more vesicles to prevent accumulation of S(0) produced by sulfide oxidation, thus playing a key role in sulfur detoxification as proposed for Archaea (30). The presence of the SurA and DegP may indicate that S(0) induces unfolded protein stress as another signal for OMV production. *Cba. tepidum* was grown on a range of sulfide concentrations (2-7 mM), and OMVs from each sulfide concentration were analyzed by MRPS. The data showed that, as sulfide concentrations are increased, particle concentration increases versus 2 mM sulfide (Fig. 5A) by 2.8-fold at 4 mM sulfide and ~10.7-fold at 5 mM, with no further significant increase at 7 mM. This result suggests that growing *Cba. tepidum* at 5 mM sulfide produced the maximum number of particles. MRPS also provides size information and documented an increase in median particle diameter from 61 nm at 2 mM sulfide to 65-67 nm at 4-5 mM while those from 7 mM cultures were 88 nm in diameter. OMV yields can be expressed in different terms, such as lipid concentration, amount of protein, total dry weight harvested, or counts by TEM, making the comparison of OMV yield using all these methods simultaneously difficult because the measurements also encompass non-vesicular materials (52, 53). TEM comparison of vesicles from 4 mM and 7 mM cultures independently confirmed the increase in OMV concentration in the 7 mM sulfide OMVs (Fig. 5 C, D). OMVs from 7 mM sulfide cultures were larger in the TEM images than those from 4 mM sulfide, but this was not significant ($p = 0.12$, t-test, 1-tailed, homoscedastic, $n = 13$ particles each). We feel the MRPS data strongly supports an increase in OMV size with increased sulfide due to the larger number of particles measured and a consistent increase of larger sizes at all sulfide concentrations in this experiment (Fig. 5B, points in the 80-110 nm range). The peak position for 7 mM may be influenced by clumping indicated by TEM (Fig. 7D), but clumping could also be a TEM sample preparation artefact. Finally, we directly compared OMVs from these samples at higher magnifications (Fig. S3) and are confident that the OMVs have the same overall structure across all samples. Collectively, these data confirm that OMV numbers and sizes vary with increased sulfide concentrations.

Molecular Composition of S(0) globules and OMVs.

The molecular composition of S(0) globules or OMVs was probed with Raman microscopy and atomic force microscopy coupled with infrared (AFM-IR) spectroscopy. Raman microscopy is a non-destructive method that gives a linear correlation of compound concentration to signal strength (31). Raman microscopic analysis of biogenic S(0) and HS-OMV samples deposited on aluminum revealed signals at 425-550 cm^{-1} (S-S, Sulfur), 580-680 cm^{-1} (C=S, thiocarbonyl), 1050-1130 cm^{-1} (carbohydrate), 1220-1290 cm^{-1} (amide III), and 1660-1680 cm^{-1} (amide I) (Fig. 6A). Different intensities of characteristic spectral regions showed that Sulfur, polysaccharides, and protein concentration were higher in S(0) globules than in HS-OMVs. S(0) may be added to a growing S(0) globule by an alternative route, possibly by excreted polysulfides as suggested by

320 Marnocha *et al.* (17). Porin proteins (e.g. OmpA and OmpH) detected in *Cba. tepidum* OMVs
321 may provide channels through which anionic polysulfide can diffuse and increase S(0)
322 concentration. Additional organic materials may also be accumulating in S(0) globules by
323 organomineralization processes (32).

324 AFM-IR spectra were collected for individual S(0) globules and OMVs. These show
325 characteristic bands for proteins (1400-1650 cm^{-1}), polysaccharides (1150-1200 cm^{-1}), and
326 sulfoxide (1030-1060 cm^{-1}) (Fig. 6b). Sulfur is an essential component of proteins; thus,
327 sulfoxide found in these samples could originate from sulfur-containing amino acids such as
328 methionine, cysteine, and homocysteine. However, Steudel *et al.* (54) collated multiple lines of
329 evidence to indicate that bacterial S(0) globules contain long-chain polythionates, which may
330 also be the source of this signature. The bands around 1650 and 1460 cm^{-1} correspond to amide I
331 and II vibrations of the peptide backbone, respectively. The presence of polysaccharides and
332 proteins is confirmed by the presence of the aliphatic group C=O bonds (around 1660 cm^{-1}) (55),
333 the weak peak around 1330-1430 cm^{-1} characteristic for a hydroxyl group, and a weak C-H peak
334 at 1370-1390 cm^{-1}. The pyranose band was observed in the regions around 1150 and 1192 cm^{-1}.
335 Though there are advantages to the usage of AFM-IR for single S(0) and OMVs characterization,
336 smaller vesicles or S(0) (15-50 nm) may not provide a strong IR signal for a consistent
337 characterization. Furthermore, the range of IR wavelengths available on the AFM IR instrument
338 was 950-1900 cm^{-1}, which would miss the strongest absorbance peaks for S-S bonds that occur
339 below 550 cm^{-1}. The Raman instrument was capable of probing this region and detected the
340 expected S-S scattering, increasing confidence in the interpretation of these data.

341 **OMVs from high sulfide cultures contain S(0).**
342 While Raman and IR spectroscopy analyses were consistent with elemental sulfur being a
343 component of HS-OMVs, the most basic question is whether purified OMVs contain elemental
344 sulfur in significant amounts. Thus, HPLC of hexane extracts was used to quantify sulfur found
345 in HS-OMVs. HPLC analysis confirmed the presence of elemental sulfur in HS-OMV (Fig. 6C)
346 that were harvested from 20 mL cultures and extracted with 1 mL of hexanes. S(0) in the HS-
347 OMV fraction was 94 $\pm$ 6 μM after accounting for the centrifugal concentration of the OMV
348 sample before extraction.
349
350 We calculated the maximum possible [S(0)] in the OMV fraction of a *Cba. tepidum* culture with
351 7 mM sulfide as follows. The particle concentration of purified OMVs at the time of sampling
352 (14 hrs) was 1.29 x 10^{12} particles/mL and the mean OMV diameter was 88 nm. The volume per
353 OMV, assuming they are spherical, is 3.82 x 10^{-16} mL. The total OMV volume per mL of culture
354 is then 4.92 x 10^{-4} mL. Different density values have been reported for biogenic S(0), 1.22 g cm^{-3}
355 (56), 1.31 g cm^{-3} (57) or 2.08 g cm^{-3} (58). Based on these values, the predicted [S(0)] if OMVs
356 were composed of solely of biogenic S(0) ranged from 18.8-32.0 mM, which is far more sulfide
357 than was provided to the culture. The observed S(0) concentration in OMVs is ~1-2% of the 7
358 mM sulfide provided to the culture, which is consistent with the hypothesis that OMVs are a

359 transient pool of S(0) with the presence of a complex proteome and LPS in these samples
360 confirming that S(0) is not the only cargo.
361
362 **Conclusions**
363 The data above clearly indicate that *Cba. tepidum*, and by extension the Chlorobiaceae,
364 synthesize LOS, secrete OMVs, and that OMVs likely contribute to material exchange between
365 cells and S(0) globules during their production and consumption. In addition, the data presented
366 here partially support our hypotheses that previously identified S(0) globule proteins would be
367 found in OMVs and that there should be substantial overlap between OMV and S(0) globule
368 proteomes. While CT1305 was found in OMVs, CT1320.1 was absent; such differences in OMV
369 protein cargo might be related to the bacterial growth stage at which OMVs were isolated or
370 difference in the proteomic sample preparation methods used. Several other pieces of evidence
371 agree with our hypotheses and indicate the roles of OMVs in sulfur metabolism: (i) OMVs and
372 S(0) globules share a substantial number of proteins; (ii) OMV abundance is higher when S(0) is
373 produced and consumed by *Cba. tepidum*; and (iii) OMVs and S(0) share a significant number of
374 chemical constituents, including elemental sulfur as documented by multiple independent
375 methods.
376
377 Taking the observations made here and by others, we propose a mechanism where *Cba. tepidum*
378 oxidizing sulfide produces OMVs to release accumulating S(0) and unfolded proteins from the
379 periplasmic space (Fig. 7). Following the accumulation of these cargos, the OM can bulge
380 outwards and pinch off as vesicles. We hypothesize that porins in the core OMV proteome (e.g.
381 e.g. OmpA/CT1353 or OmpH/CT0254) in the growing S(0) globules may also allow for
382 additional S(0) to accumulate perhaps by diffusion of polysulfides from cells. Clearly, additional
383 mechanisms of transport and/or globule maturation occur, otherwise the chemical and proteome
384 compositions of OMVs and S(0) globules would be nearly identical. Previous measurements of
385 *Cba. tepidum* S(0) globule elemental composition indicate that they are > 99% S (1). A
386 maturation process may explain why purified S(0) globules contain higher relative amounts of S,
387 polysaccharides, and amides than OMVs based on the IR and Raman spectroscopy data
388 presented above. A simple possibility could be the exclusion or expulsion of water and
389 hydrophilic OMV cargos if multiple S(0) payloads condense by hydrophobic attraction.
390 Experiments to observe OMV fusion and S(0) globule maturation in over time from purified
391 OMVs and determining if S(0)-loaded OMVs can be used for growth by *Cba. tepidum* are
392 obvious next steps to further dissect this process.
393
394 **MATERIALS AND METHODS**
395 **Bacterial strain and growth conditions**
396 *Cba. tepidum* strain WT2321 was used in all cultures and grown in Pfennig's (Pf-7) medium, as
397 previously described by (59) with an anaerobic headspace composed of 5% CO_2 and 95% N_2
398 passed through a heated copper scrubber. *Cba. tepidum* cultures used for OMVs isolation were

399 incubated at 47°C with light provided by incandescent bulbs at an intensity of 20 µmol photons
400 m^{-2} s^{-1} measured with a light meter equipped with a quantum PAR sensor (LI-COR, Lincoln,
401 NE). *Cba. tepidum* liquid cultures were grown to different growth phases as noted in figure
402 legends. Electron donors (sulfide or thiosulfate) were added to individual bottles from
403 concentrated, anoxic stock solutions for biogenic S(0), sulfide and thiosulfate-only cultures.
404 Other growth conditions, such as light intensity and temperature, remained unchanged.
405
406 **Extracellular particle isolation and purification**
407 Extracellular particles were isolated and purified by differential centrifugation (53). One liter of
408 *Cba. tepidum* culture was centrifuged at 10,000 x *g* for 10 min at 4°C in a JA-14 rotor (Beckman
409 Coulter), and the supernatant was centrifuged again at 12,000 x *g* to remove cells and large
410 debris. The supernatant was filtered through a 0.22-µm pore-size polyvinylidene difluoride
411 (PVDF) filter membrane (Millipore, USA). Particles from the filtrate were concentrated by
412 ultracentrifugation at 100,000 x *g* for 2 h at 4°C using an SW32Ti rotor in an Optima LE-80K
413 centrifuge (Beckman Coulter). The pellets from different centrifuge tubes were pooled and
414 resuspended in 1 mL of 1X PBS and pelleted again by ultracentrifugation at 165,700 x *g* for 2 h
415 at 4°C in a TLA-55 rotor (Beckman Coulter). The pellet was resuspended in 500 µL of 1X PBS
416 and stored at -20°C until use. The total protein concentration of purified OMVs was determined
417 using the fluorometric Qubit protein assay (ThermoFisher Scientific) according to the
418 manufacturer's guidelines.
419
420 **Particle characterization by MRPS**
421 Particle samples for quantification from cultures were prepared by centrifugation through a 0.2
422 µm filter device at 16,000 x *g* for 2 minutes in an Eppendorf 5418 centrifuge. The flow through
423 was used diluted 100-fold with 0.02 µm filtered 1X PBS with 0.1% w/v BSA before analysis.
424 MRPS was performed using an nCS1 instrument (Spectradyne, Torrance, CA, USA) equipped
425 with disposable polydimethylsiloxane cartridges (mold ID 103S and box number 221118). The
426 running buffer was 0.2 µm filtered 1X PBS with 1% (v/v) Tween-20. Diluted OMV samples (7
427 µL) were loaded, and the particle detection threshold was set after three 10-s acquisitions. Data
428 was collected until the error associated with the concentration measurement was < 3%. The
429 collected data were analyzed with nCS1 Data Analyzer software (Spectradyne). The particle
430 distribution of the dilution buffer was also measured and subtracted from OMV sample data to
431 produce the OMV size and frequency distributions shown. Examples of raw nCS1 particle count
432 data are provided in supplemental materials (Fig. S4).
433
434 **Electron microscopic imaging of purified particles**
435 The particle suspension from *Cba. tepidum* was negatively stained with aqueous 2% (w/v) uranyl
436 acetate. Briefly, 400-mesh carbon-coated copper grids (Electron Microscopy Sciences) were
437 glow discharged using a PELCO easiGlow™ glow discharge system (Ted Pella) and then floated
438 on a drop of the vesicle suspension for several seconds. The grids were washed with four drops

439 of water and then negatively stained with aqueous 2% uranyl acetate. Samples were examined in
440 the bioimaging core facility at the University of Delaware using a Zeiss Libra 120 TEM
441 equipped with a Gatan Ultrascan1000 CCD (Fig. 2) or a Thermo Scientific Talos L120C TEM
442 equipped with a Thermo Scientific Ceta-M camera (Fig. 5). For each analysis, at least 15 fields
443 were imaged. To examine particles attached to cells, *Cba. tepidum* culture fixed with 0.4%
444 formaldehyde was centrifuged at 10,000 x *g* for 5 minutes, the supernatant was removed, and the
445 pellet was processed for TEM imaging as described above. Particle size was determined by
446 analysis with ImageJ software (v1.54g). ImageJ was also used to select and scale individual
447 regions of interest from different experiments to the same magnification to compare particle
448 structure across experiments (Fig. S3).
449
450 **LPS purification and analysis**
451 LPS was extracted from a suspension of 4×10^{10} particles mL^{-1} by a previously described method
452 (60). LPS was separated by SDS-PAGE using 16% Tricine protein gels (1.0 mm, 14 wells,
453 BioRad) and Tricine SDS running buffer with LPS from *E. coli* O55:B5 as a standard
454 (InvivoGen). The gel was run at 125 V for 120 min at room temperature and stained with Pro-Q
455 Emerald 300 (Thermo Fisher) per the manufacturer's instructions. Briefly, the gel was oxidized
456 with periodic acid and then washed with 3% glacial acetic to remove residual periodate. The gel
457 was then incubated in 25-fold diluted Pro-Q Emerald 300 staining solution. Gel images were
458 collected on a BioRad ChemiDoc system using Image Lab software version 5.0. Images were
459 automatically contrast adjusted by the software and exported as a TIFF file to produce the figures
460 here.
461
462 **Mass spectrometry of lipid A**
463 Mild acid hydrolysis was used to separate lipid A from LPS/LOS by resuspending 0.6 mg of
464 lyophilized purified LPS in 1 mL sodium acetate (10 mM, pH = 4.5) and 1% w/v sodium
465 dodecyl sulfate (SDS). The suspension was boiled (100 ºC, 1h) and then lyophilized. Lyophilized
466 material was washed once with 1 mL of ice-cold acidified ethanol, followed by three washes
467 with ice-cold 95% ethanol to remove SDS from the solid material collected by centrifugation
468 (3,500 x *g*; 4 ºC; 5 min). The final lipid A samples were lyophilized before analysis by mass
469 spectrometry. Samples were reconstituted in 10 uL methanol, then diluted into 5:4:1
470 chloroform:methanol:water. Lipid A analysis was performed on an UltiMate 3000 UPLC system
471 coupled with an Orbitrap Q-Exactive (Thermo Fisher Scientific) mass spectrometer. A 5 µL
472 sample was injected by syringe at a flow rate of 0.2 mL/min, with the column temperature set at
473 40 °C. Samples were separated in isocratic mode (50:50 0.1% (v/v) formic acid in LC-MS grade
474 H_2O:0.1% (v/v) formic acid in LC-MS grade acetonitrile). After separation, the mass
475 spectrometry data were acquired on a Q-Exactive Orbitrap (Thermo Fisher Scientific) equipped
476 with heated electrospray ionization (HESI-II) operating in negative ionization mode. The HESI-
477 II was maintained at a spray voltage of -3.5 kV, and the mass range was set from 600-2200 m/z.
478 Data were processed using Thermo Scientific Xcalibur software version 3.1 (Thermo Fisher

479 Scientific). The lipid A molecular species were identified based on using observed mass to
480 charge (m/z) ratios to search the Lipid MAPS databases (61).
481
482 **Quantification of 2-Keto-3-Deoxy-D-Mannooctanoic Acid (KDO)**
483 KDO was derivatized with 1,2-diamino-4,5-methylenedioxybenzene dihydrochloride (DMB,
484 Sigma-Aldrich), and the resulting derivatives were quantified by HPLC following a previously
485 described method (62). Briefly, a KDO standard (Sigma-Aldrich), and purified LPS samples
486 were hydrolyzed using trifluoroacetic acid (TFA). DMB solution (5 mM, 125 mL) prepared
487 according to Hara et al., 1987 (63) was added to hydrolyzed samples, and the mixture was placed
488 in a heat block (50 ºC, 2.5 hrs) covered with aluminum foil. Subsequently, samples were placed
489 on ice (10 min), centrifuged (5 min, 10,000 rpm, 4 ºC), and analyzed using a Shimadzu SCL-40
490 HPLC system. A Prevail C18 (150 x 4.6 mm, 5 µm particle size, Alltech) analytical column was
491 used; 10 µL of sample was injected; separation was in isocratic mode (86% of 0.1%TFA, 7%
492 Acetonitrile, and 7% Methanol) at 1.3 mL min^{-1} for 20 min. DMB derivatives were detected by
493 fluorescence with excitation at 373 nm and emission at 448 nm.
494
495 **Raman Microscopy-Spectroscopy**
496 Samples (40 µL) of S(0) globules or OMVs in 1X PBS were pipetted onto aluminum foil held by
497 an HPLC screw top cap taped to a microscope slide and allowed to dry. Aluminum foil is a non-
498 reactive substrate for Raman measurements. A confocal Raman microscope (LabRam HR
499 Evolution, Horiba Scientific, Kyoto, Japan) was used to record data at the Surface Analysis
500 Facility, University of Delaware. A 532-nm laser was used, and the laser power applied was set
501 at 100%, which corresponds to a laser power of 20 mW on samples. Raman Spectra were
502 obtained over 5 seconds of acquisition time with a wavenumber from 400-4000 cm^{-1} with six
503 accumulations per spectrum.
504
505 **Combined Atomic Force Microscopy and Infrared Spectroscopy (AFM-IR)**
506 AFM-IR analysis was performed with a NanoIR2 instrument (Anasys Instruments, Santa
507 Barbara, CA, USA, now Bruker) at the Advanced Materials Characterization Laboratory,
508 University of Delaware. A 5 µL aliquot of samples was spread on a zinc sulfide sampling flat
509 and placed on the stage of the AFM-IR instrument. All AFM-IR measurements and images were
510 done under contact mode. A 1 µm × 1 µm scan area was imaged at a scan rate of 0.6 Hz with a
511 resolution of 384 pixels in both x and y axes. Individual AFM-IR spectra were collected using a
512 MIRcat-2400 laser (Daylight Solutions, San Diego, CA, USA) across the 950-1900 cm^{-1}
513 frequency range. The IR laser produced pulses of 140 ns at the repetition rate of 350 kHz.
514 Analysis Studio software (Anasys Instruments, Santa Barbara, CA, USA) was used for image
515 and spectral data collection.

516 **S(0) Globule Purification**
517 Cultures (1 L) of strain WT2321 were grown on sulfide-only Pf-7 (4 mM sulfide) in narrow-
518 mouth screw-cap bottles with an open phenolic cap and butyl rubber septa at 30 µmol photon m^{-2}

519 s^{-1} for 36 h. To qualitatively assay for the presence of sulfide, equal volumes of culture
520 supernatant were mixed with 10 mM $CuCl_2$, where the formation of a distinct grey precipitate
521 indicated the presence of sulfide greater than 0.2 mM. Sulfide was added to cultures when it was
522 no longer detectable by this assay. Cultures were transferred into sterile 250 ml centrifuge bottles
523 with o-ring sealing caps (Nalgene, Thermo Fisher Scientific). Cells and S(0) were collected by
524 centrifugation (1,000 × *g*, 10 min, 10 °C, JA-14 rotor). The supernatant was removed and cells
525 plus S(0) were suspended in a minimal volume of S-free Pf-7 that was layered over 25 ml of
526 sterile 2.5 M sucrose solution in sterile 50 ml centrifuge tubes with o-ring sealing caps (Nalgene,
527 Thermo Fisher Scientific); at a density of 1.32 g ml^{-1}, the sucrose retains cells in the supernatant
528 and selectively pellets S(0) when centrifuged (6,000 × *g,* 50 min, 4 °C, JS-13.1 rotor). The
529 supernatant was removed, and the resuspended pellet was centrifuged through 2.5 M sucrose two
530 more times. The collected S(0) pellet was washed three times to remove sucrose by suspending
531 in S-free Pf-7 and centrifuging (17,500 × *g* , 5 min, 10 °C, JS-13.1 rotor). S(0) was suspended in
532 S-free Pf-7 and immediately distributed into aliquots for characterization studies; aliquots were
533 stored at -80 °C until use.
534
535 **Proteomic profiling of OMVs, S(0) globules, and whole cells**
536 Purified OMVs, S(0) globules and whole cell pellets were dissolved in SDS buffer (2% SDS, 50
537 mM DTT, and 100 mM Tris-HCl pH 8.0) and sonicated for 3 min (pulse: 20s on, 20s off). After
538 sonication, the suspension was incubated at 95 ºC for 10 min. A clear lysate was obtained after
539 centrifugation (16,000 x *g*, 10 min, 25 ºC, Eppendorf 5415 centrifuge). Proteins in the lysate
540 were processed for proteomics analysis following the E3 filter procedure described recently (64).
541 The digests were desalted using C18-based StageTips (CDS Analytical, Oxford, PA). Liquid
542 chromatography-tandem mass spectrometry (LC-MS/MS) was performed on an Ultimate 3000
543 nanoLC system coupled to an Orbitrap Eclipse Tribrid mass spectrometer with FAIMS Interface
544 (Thermo Scientific). Peptides were separated on a C18 reversed phase column (PepMap100 C18,
545 25 cm × 75 µm i.d., 3 µm; Thermo Scientific) at a flow rate of 250 nl/min. Mobile phase A
546 consisted of 0.1% formic acid in water. Mobile phase B consisted of 0.1% formic acid in
547 acetonitrile. A gradient separation was used: mobile phase B was held at 1% for 5 min, increased
548 to 25% over 90 min, reached to 35% at 110 min, increased to 80% over 10 min, then re-
549 equilibrated at 1% mobile phase B for 15 min. For data-dependent MS acquisition, the spray
550 voltage was set to 1.8 kV, funnel RF level at 50%, and heated capillary temperature at 275 °C.
551 The MS data were acquired in Orbitrap mode at 60,000 resolution, followed by MS/MS
552 acquisition of the most intense precursors for 1 s. For MS2 analysis, collision was set by HCD at
553 30% normalized collision energy (NCE). For FAIMS settings, a 3-CV experiment (-40|-55|-75)
554 was applied.

555 Peptide identification and quantitation used MaxQuant and Andromeda software (version
556 1.6.3.4) with most default settings. *Cba. tepidum* proteome database (Taxon ID 194439; 2,251
557 sequences) was obtained from UniProt Knowledgebase. The enzyme specificity was set to
558 'Trypsin'; oxidation of methionine, and acetyl (protein N-terminus) were set as variable

559 modification; carbamidomethylation of cysteine was set as fixed modification. Up to 2 missed
560 cleavages were allowed. The false discovery rate (FDR) was set to 1% for protein and peptide
561 identifications. MaxLFQ function embedded in MaxQuant was enabled for label-free
562 quantitation, and the LFQ minimum ratio count set to 1.

563 **Bioinformatic classification of identified proteins**

564 Visualization of quantitative proteomic data was mainly performed using Perseus software
565 (version 1.6.2.3) (65). Label-free quantitation intensities generated by MaxQuant were log2-
566 transformed and imported into Perseus with protein annotations. As noted in the Results, the
567 thiosulfate OMV samples were removed, and data were filtered to only contain proteins observed
568 in at least 2/12 samples (n = 1,447 unique proteins). Uniprot accessions for proteins associated
569 with each sample type were exported for to FunRich v. 3.1.3 (66) to construct a Venn diagram
570 (Fig. 4A). NaNs were replaced using randomly selected values from a normal distribution with
571 the default settings (downshift value = 1.8 standard deviations, width = 0.3). The NaN replaced
572 data were used for principal component analysis (PCA). The PCA scores and loadings for each
573 protein were exported from Perseus to Excel to produce the plots (Fig. 4B and 4C) The
574 subcellular localization of each protein was predicted using the PSORTb subcellular localization
575 tool version 3.0.3 (https://www.psort.org/psortb/) and merged with the data from Perseus in
576 Excel to color loading values of individual proteins based on predicted localization (Fig. 4B).
577 The Perseus session file and Excel file containing all data in Figure 4 are available at:
578 https://hansonlabgit.dbi.udel.edu/hanson/ctep_omv_manuscript
579

580 **S(0) Quantification in OMVs**

581 Three independent 20 mL cultures of *Cba. tepidum* were grown with 7 mM sulfide for 14 hrs.
582 OMVs were purified from the entire volume of each culture as above and resuspended in 20
583 microL of 1X PBS after the second ultracentrifugation. A 15 microL aliquot of OMV suspension
584 was extracted with 1 mL of hexanes (Sigma Aldrich). S(0) was quantified in the hexane phase by
585 HPLC on a 4.6 x 150 mM Prevail C18 column eluted with 90% methanol at 1 mL min^{-1}
586 following absorbance at 280 nm on a Shimadzu SCL-40 HPLC system. Sulfur powder (Sigma-
587 Aldrich) dissolved in chloroform was diluted to known concentrations in hexane to generate a
588 standard curve. The remaining OMV suspension was used for TEM imaging as described above.
589

590 **ACKNOWLEDGMENTS**

591 This research was partially supported by a National Science Foundation research grant to TEH
592 (1244373). VLN was partially supported by a grant from the W.M. Keck Foundation
593 (16A01455). ATL was supported by an NSF Graduate Research Fellowship Program award
594 (0750966). Research reported in this publication was supported by the National Institute of
595 General Medical Sciences of the National Institutes of Health under Award Numbers
596 T32GM133395 (partial support for VLN) and P20GM104316 for the Orbitrap Eclipse MS
597 instrument. Microscopy equipment was acquired with Unidel Foundation support and a Major
598 Research Instrumentation award (1828325) for the purchase of the LabRam HR Evolution.

599 Microscopy access was supported by grants from the NIH-NIGMS (P20GM103446), the
600 NIGMS (P20GM139760) and the State of Delaware. The content is solely the responsibility of
601 the authors and does not necessarily represent the official views of the W.M. Keck Foundation,
602 the National Institutes of Health, or the National Science Foundation.
603

604 **CONFLICT OF INTEREST DISCLOSURE**

605 Y.Y. is a named inventor on a patent application (PCT/US2023/020215) for the E3 technology,
606 which has been licensed exclusively to CDS Analytical LLC (Oxford, PA).

607 **REFERENCES**

608 1. Hanson TE, Bonsu E, Tuerk A, Marnocha CL, Powell DH, Chan CS. 2016. *Chlorobaculum*
609 *tepidum* growth on biogenic S(0) as the sole photosynthetic electron donor. Environ
610 Microbiol 18:2856–2867.

611 2. Gralnick JA, Bond DR. 2023. Electron transfer beyond the outer membrane: Putting
612 electrons to rest. Annu Rev Microbiol 77:517–539.

613 3. Beblawy S, Bursac T, Paquete C, Louro R, Clarke TA, Gescher J. 2018. Extracellular
614 reduction of solid electron acceptors by *Shewanella oneidensis*. Mol Microbiol 109:571–
615 583.

616 4. Gadd GM. 2010. Metals, minerals and microbes: geomicrobiology and bioremediation.
617 Microbiology 156:609–643.

618 5. Schertzer JW, Whiteley M. 2013. Bacterial outer membrane vesicles in trafficking,
619 communication and the host-pathogen interaction. J Mol Microbiol Biotechnol 23:118–130.

620 6. Dhurve G, Madikonda AK, Jagannadham MV, Siddavattam D. 2022. Outer membrane
621 vesicles of *Acinetobacter baumannii* DS002 are selectively enriched with TonB-dependent
622 transporters and play a key role in iron acquisition. Microbiol Spectr 10:e0029322.

623 7. Clark MM, Paxhia MD, Young JM, Manzella MP, Reguera G. 2021. Adaptive synthesis of a
624 rough lipopolysaccharide in *Geobacter sulfurreducens* for metal reduction and
625 detoxification. Appl Environ Microbiol AEM0096421.

626 8. Wahlund TM, Woese CR, Castenholz RW, Madigan MT. 1991. A thermophilic green sulfur
627 bacterium from New Zealand hot springs, *Chlorobium tepidum* sp. nov.. Arch Microbiol
628 156:81–90.

629 9. Eisen JA, Nelson KE, Paulsen IT, Heidelberg JF, Wu M, Dodson RJ, Deboy R, Gwinn ML,
630 Nelson WC, Haft DH, Hickey EK, Peterson JD, Durkin AS, Kolonay JL, Yang F, Holt I,
631 Umayam LA, Mason T, Brenner M, Shea TP, Parksey D, Nierman WC, Feldblyum TV,
632 Hansen CL, Craven MB, Radune D, Vamathevan J, Khouri H, White O, Gruber TM,
633 Ketchum KA, Venter JC, Tettelin H, Bryant DA, Fraser CM. 2002. The complete genome
634 sequence of *Chlorobium tepidum* TLS, a photosynthetic, anaerobic, green-sulfur bacterium.
635 Proc Natl Acad Sci U S A 99:9509–9514.

636 10. Frigaard NU, Bryant DA. 2001. Chromosomal gene inactivation in the green sulfur
637 bacterium *Chlorobium tepidum* by natural transformation. Appl Environ Microbiol
638 67:2538–2544.

639 11. Hanson TE, Tabita FR. 2001. A ribulose-1,5-bisphosphate carboxylase/oxygenase
640 (RubisCO)-like protein from *Chlorobium tepidum* that is involved with sulfur metabolism
641 and the response to oxidative stress. Proc Natl Acad Sci U S A 98:4397–4402.

642 12. Maresca JA, Gomez Maqueo Chew A, Ponsatí MR, Frigaard N-U, Ormerod JG, Bryant DA.
643 2004. The *bchU* gene of *Chlorobium tepidum* encodes the C-20 methyltransferase in
644 bacteriochlorophyll *c* biosynthesis. J Bacteriol 186:2558–2566.

645 13. Evans BYMC, Buchanan BB, Arnon DI. 1966. A new ferredoxin-dependent carbon
646 reduction cycle in a photosynthetic bacterium. Proc Natl Acad Sci U S A 55:928–934.

647 14. Wahlund TM, Tabita FR. 1997. The reductive tricarboxylic acid cycle of carbon dioxide
648 assimilation: initial studies and purification of ATP-citrate lyase from the green sulfur
649 bacterium *Chlorobium tepidum*. J Bacteriol 179:4859–4867.

650 15. Chan L-K, Morgan-Kiss RM, Hanson TE. 2009. Functional analysis of three
651 sulfide:quinone oxidoreductase homologs in *Chlorobaculum tepidum*. J Bacteriol
652 191:1026–1034.

653 16. Shuman KE, Hanson TE. 2016. A sulfide:quinone oxidoreductase from *Chlorobaculum*
654 *tepidum* displays unusual kinetic properties. FEMS Microbiol Lett 363.

655 17. Marnocha CL, Levy AT, Powell DH, Hanson TE, Chan CS. 2016. Mechanisms of
656 extracellular S0 globule production and degradation in *Chlorobaculum tepidum* via dynamic
657 cell-globule interactions. Microbiology 162:1125–1134.

658 18. Reguera G, Kashefi K. 2019. The electrifying physiology of *Geobacter* bacteria, 30 years
659 on. Adv Microb Physiol 74:1–96.

660 19. Lyratzakis A, Meier-Credo J, Langer JD, Tsiotis G. 2023. Insights into the sulfur
661 metabolism of *Chlorobaculum tepidum* by label-free quantitative proteomics. Proteomics
662 e2200138.

663 20. Marnocha CL, Sabanayagam CR, Modla S, Powell DH, Henri PA, Steele AS, Hanson TE,
664 Webb SM, Chan CS. 2019. Insights into the mineralogy and surface chemistry of
665 extracellular biogenic S0 globules produced by *Chlorobaculum tepidum*. Front Microbiol
666 10:271.

667 21. Beveridge TJ. 1999. Structures of gram-negative cell walls and their derived membrane
668 vesicles. J Bacteriol 181:4725–4733.

669 22. Lee E-Y, Choi D-S, Kim K-P, Gho YS. 2008. Proteomics in gram-negative bacterial outer
670 membrane vesicles. Mass Spectrom Rev 27:535–555.

671 23. Veith PD, Chen Y-Y, Gorasia DG, Chen D, Glew MD, O'Brien-Simpson NM, Cecil JD,
672 Holden JA, Reynolds EC. 2014. *Porphyromonas gingivalis* outer membrane vesicles
673 exclusively contain outer membrane and periplasmic proteins and carry a cargo enriched
674 with virulence factors. J Proteome Res 13:2420–2432.

675 24. Balhuizen MD, Veldhuizen EJA, Haagsman HP. 2021. Outer membrane vesicle induction
676 and isolation for vaccine development. Front Microbiol 12:629090.

677 25. Mause SF, Weber C. 2010. Microparticles: Protagonists of a novel communication network
678 for intercellular information exchange. Circ Res 107:1047–1057.

679 26. Caruana JC, Walper SA. 2020. Bacterial membrane vesicles as mediators of microbe -
680 microbe and microbe - host community interactions. Front Microbiol 11:432.

681 27. Cron B, Henri P, Chan CS, Macalady JL, Cosmidis J. 2019. Elemental sulfur formation by
682 *Sulfuricurvum kujiense* is mediated by extracellular organic compounds. Front Microbiol
683 10:2710.

684 28. Cosmidis J, Templeton AS. 2016. Self-assembly of biomorphic carbon/sulfur
685 microstructures in sulfidic environments. Nat Commun 7:12812.

686 29. Li W, Zhu L, Pan C, Chen W, Xu D, Kang D, Guo L, Mei Q, Zheng P, Zhang M. 2023.
687 Insights into the superior bioavailability of biogenic Sulfur from the view of its unique
688 properties: The key role of trace organic substances. Environ Sci Technol **57**:1487–1498.

689 30. Gorlas A, Marguet E, Gill S, Geslin C, Guigner J-M, Guyot F, Forterre P. 2015. Sulfur
690 vesicles from Thermococcales: A possible role in sulfur detoxifying mechanisms. Biochimie
691 118:356–364.

692 31. Nims C, Cron B, Wetherington M, Macalady J, Cosmidis J. 2019. Low frequency Raman
693 Spectroscopy for micron-scale and in vivo characterization of elemental sulfur in microbial
694 samples. Sci Rep 9:7971.

695 32. Cosmidis J, Nims CW, Diercks D, Templeton AS. 2019. Formation and stabilization of
696 elemental sulfur through organomineralization. Geochim Cosmochim Acta 247:59–82.

697 33. Kulp A, Kuehn MJ. 2010. Biological functions and biogenesis of secreted bacterial outer
698 membrane vesicles. Annu Rev Microbiol 64:163–184.

699 34. Yáñez-Mó M, Siljander PR-M, Andreu Z, Zavec AB, Borràs FE, Buzas EI, Buzas K, Casal
700 E, Cappello F, Carvalho J, Colás E, Cordeiro-da Silva A, Fais S, Falcon-Perez JM, Ghobrial
701 IM, Giebel B, Gimona M, Graner M, Gursel I, Gursel M, Heegaard NHH, Hendrix A,
702 Kierulf P, Kokubun K, Kosanovic M, Kralj-Iglic V, Krämer-Albers E-M, Laitinen S, Lässer
703 C, Lener T, Ligeti E, Linē A, Lipps G, Llorente A, Lötvall J, Manček-Keber M, Marcilla A,
704 Mittelbrunn M, Nazarenko I, Nolte-'t Hoen ENM, Nyman TA, O'Driscoll L, Olivan M,
705 Oliveira C, Pállinger É, Del Portillo HA, Reventós J, Rigau M, Rohde E, Sammar M,
706 Sánchez-Madrid F, Santarém N, Schallmoser K, Ostenfeld MS, Stoorvogel W, Stukelj R,
707 Van der Grein SG, Vasconcelos MH, Wauben MHM, De Wever O. 2015. Biological
708 properties of extracellular vesicles and their physiological functions. J Extracell Vesicles
709 4:27066.

710 35. Parks DH, Chuvochina M, Waite DW, Rinke C, Skarshewski A, Chaumeil P-A, Hugenholtz
711 P. 2018. A standardized bacterial taxonomy based on genome phylogeny substantially
712 revises the tree of life. Nat Biotechnol 36:996–1004.

713 36. Hug LA, Baker BJ, Anantharaman K, Brown CT, Probst AJ, Castelle CJ, Butterfield CN,
714 Hernsdorf AW, Amano Y, Ise K, Suzuki Y, Dudek N, Relman DA, Finstad KM, Amundson
715 R, Thomas BC, Banfield JF. 2016. A new view of the tree of life. Nat Microbiol 1:16048.

716 37. Oren A, Garrity GM. 2021. Valid publication of the names of forty-two phyla of
717 prokaryotes. Int J Syst Evol Microbiol 71.

718 38. McCaig WD, Koller A, Thanassi DG. 2013. Production of outer membrane vesicles and
719 outer membrane tubes by *Francisella novicida*. J Bacteriol 195:1120–1132.

720 39. Sharif E, Eftekhari Z, Mohit E. 2021. The effect of growth stage and isolation method on
721 properties of ClearColi^{TM} outer membrane vesicles (OMVs). Curr Microbiol 78:1602–1614.

722 40. Zavan L, Bitto NJ, Johnston EL, Greening DW, Kaparakis-Liaskos M. 2019. *Helicobacter*
723 *pylori* growth stage determines the size, protein composition, and preferential cargo
724 packaging of outer membrane vesicles. Proteomics 19:e1800209.

725 41. Siegele DA, Kolter R. 1992. Life after log. J Bacteriol 174:345–348.

726 42. Monod J. 1949. The growth of bacterial cultures. Annu Rev Microbiol 3:371–394.

727 43. Lewis K. 2000. Programmed death in bacteria. Microbiol Mol Biol Rev 64:503–514.

728 44. Jacobson AN, Choudhury BP, Fischbach MA. 2018. The biosynthesis of lipooligosaccharide
729 from *Bacteroides thetaiotaomicron*. MBio 9:10.1128/mbio.02289-17. 45. Meißner J,
730 Fischer U, Weckesser J. 1987. The lipopolysaccharide of the green sulfur bacterium
731 *Chlorobium vibrioforme* f. *thiosulfatophilum*. Arch Microbiol 149:125–129.

732 46. Bonnington KE, Kuehn MJ. 2016. Outer membrane vesicle production facilitates LPS
733 remodeling and outer membrane maintenance in *Salmonella* during environmental
734 transitions. MBio 7.

735 47. Sartorio MG, Pardue EJ, Feldman MF, Haurat MF. 2021. Bacterial outer membrane
736 vesicles: From discovery to applications. Annu Rev Microbiol 75:609–630.

737 48. Elhenawy W, Bording-Jorgensen M, Valguarnera E, Haurat MF, Wine E, Feldman MF.
738 2016. LPS remodeling triggers formation of outer membrane vesicles in *Salmonella*. MBio
739 7:10.1128/mbio.01532-16.

740 49. Liu X, Jing X, Ye Y, Zhan J, Ye J, Zhou S. 2020. Bacterial vesicles mediate extracellular
741 electron transfer. Environ Sci Technol Lett 7:27–34.

742 50. Sklar JG, Wu T, Kahne D, Silhavy TJ. 2007. Defining the roles of the periplasmic
743 chaperones SurA, Skp, and DegP in *Escherichia coli*. Genes Dev 21:2473–2484.

744 51. Costello SM, Plummer AM, Fleming PJ, Fleming KG. 2016. Dynamic periplasmic
745 chaperone reservoir facilitates biogenesis of outer membrane proteins. Proc Natl Acad Sci U
746 S A 113:E4794–E4800.

747 52. Li M, Zhou H, Yang C, Wu Y, Zhou X, Liu H, Wang Y. 2020. Bacterial outer membrane
748 vesicles as a platform for biomedical applications: An update. J Control Release 323:253–
749 268.

750 53. Klimentová J, Stulík J. 2015. Methods of isolation and purification of outer membrane
751 vesicles from gram-negative bacteria. Microbiol Res 170:1–9.

752 54. Steudel R, Holdt G, Göbel T, Hazeu W. 1987. Chromatographic separation of higher
753 polythionates $S_nO_6^{2-}$(n= 3…22) and their detection in cultures of *Thiobacillus ferroxidans*;
754 Molecular composition of bacterial sulfur secretions. Angew Chem Int Ed Engl 26:151–
755 153.

756 55. Freddi G, Tsukada M, Beretta S. 1999. Structure and physical properties of silk
757 fibroin/polyacrylamide blend films. J Appl Polym Sci 71:1563–1571.

758 56. Guerrero R, Mas J, Pedrós-Alió C. 1984. Buoyant density changes due to intracellular
759 content of sulfur in *Chromatium warmingii* and *Chromatium vinosum*. Arch Microbiol
760 137:350–356.

761 57. Mas J, van Gemerden H. 1987. Influence of sulfur accumulation and composition of sulfur
762 globule on cell volume and buoyant density of *Chromatium vinosum*. Arch Microbiol
763 146:362–369.

764 58. Meyer B. 1976. Elemental sulfur. Chem Rev 76:367–388.

765 59. Chan L-K, Weber TS, Morgan-Kiss RM, Hanson TE. 2008. A genomic region required for
766 phototrophic thiosulfate oxidation in the green sulfur bacterium *Chlorobium tepidum* (syn.
767 *Chlorobaculum tepidum*). Microbiology 154:818–829.

768 60. Yi EC, Hackett M. 2000. Rapid isolation method for lipopolysaccharide and lipid A from
769 gram-negative bacteria. Analyst 125:651–656.

770 61. Sud M, Fahy E, Cotter D, Brown A, Dennis EA, Glass CK, Merrill AH Jr, Murphy RC,
771 Raetz CRH, Russell DW, Subramaniam S. 2007. LMSD: LIPID MAPS structure database.
772 Nucleic Acids Res 35:D527-32.

773 62. Bucsella B, Hoffmann A, Zollinger M, Stephan F, Pattky M, Daumke R, Heiligtag FJ, Frank
774 B, Bassas-Galia M, Zinn M, Kalman F. 2020. Novel RP-HPLC based assay for selective
775 and sensitive endotoxin quantification. Anal Methods 12:4621–4634.

776 63. Hara S, Yamaguchi M, Takemori Y, Furuhata K, Ogura H, Nakamura M. 1989.
777 Determination of mono-O-acetylated N-acetylneuraminic acids in human and rat sera by
778 fluorometric high-performance liquid chromatography. Anal Biochem 179:162–166.

779 64. Martin KR, Le HT, Abdelgawad A, Yang C, Lu G, Keffer JL, Zhang X, Zhuang Z, Asare-
780 Okai PN, Chan CS, Batish M, Yu Y. 2024. Development of an efficient, effective, and
781 economical technology for proteome analysis. Cell Rep Methods 4:100796.

782 65. Tyanova S, Temu T, Sinitcyn P, Carlson A, Hein MY, Geiger T, Mann M, Cox J. 2016. The
783 Perseus computational platform for comprehensive analysis of (prote)omics data. Nat
784 Methods 13:731–740.

785 66. Pathan M, Keerthikumar S, Ang C-S, Gangoda L, Quek CYJ, Williamson NA, Mouradov
786 D, Sieber OM, Simpson RJ, Salim A, Bacic A, Hill AF, Stroud DA, Ryan MT, Agbinya JI,
787 Mariadason JM, Burgess AW, Mathivanan S. 2015. FunRich: An open access standalone
788 functional enrichment and interaction network analysis tool. Proteomics 15:2597–2601.

789

790

791 **FIGURES**

792

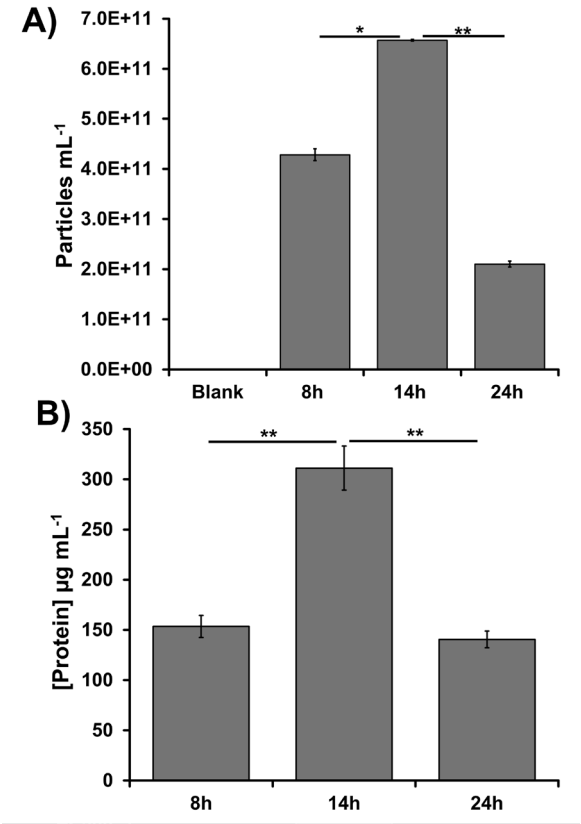

Figure 1. The effect of *Cba. tepidum* growth phase on extracellular particle concentration in cultures and protein concentration in purified particle preparations. See Fig. S1A for details on purification. **A)** Extracellular particles concentration from different growth phases. **B)** Total protein concentration of particles purified at different growth phases. Error bars represent the standard error, n = 3 with * indication $p < 0.05$ and ** indicating $p < 0.01$ (t-test, two tailed, unequal variance).

793

794

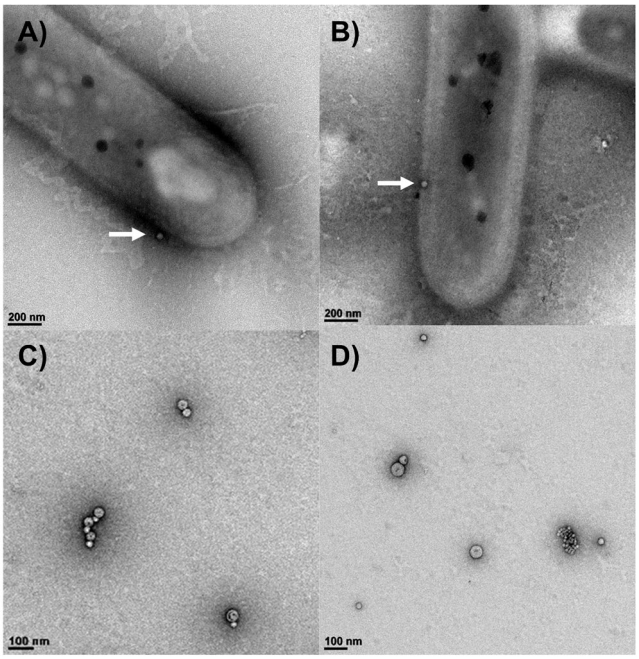

Figure 2. Transmission electron microscopy (TEM) images of *Cba. tepidum*'s OMVs. **A)** and **B)** TEM images show spherical OMVs budding out of rod-shaped *Cba. tepidum* after 8h and 14h of growth, respectively (white arrows). **C)** and **D)** TEM analysis of OMVs purified via serial ultracentrifugation from a 14 h old *Cba. tepidum* culture.

795

796

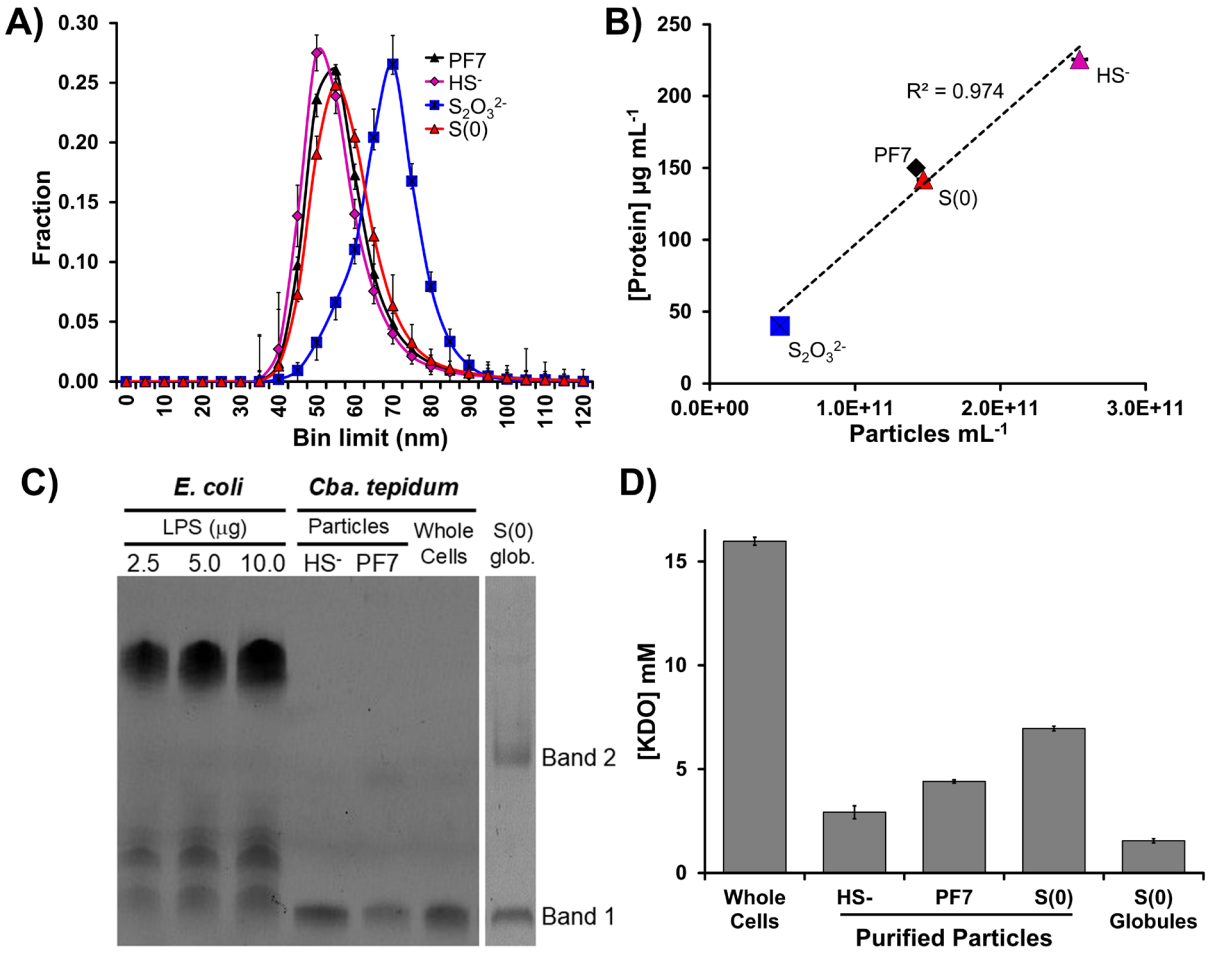

Figure 3. Analysis of *Cba. tepidum* extracellular particles for hallmark characteristics of OMVs including size (A), protein (B), LPS or LOS (C), KDO (D).

797

798

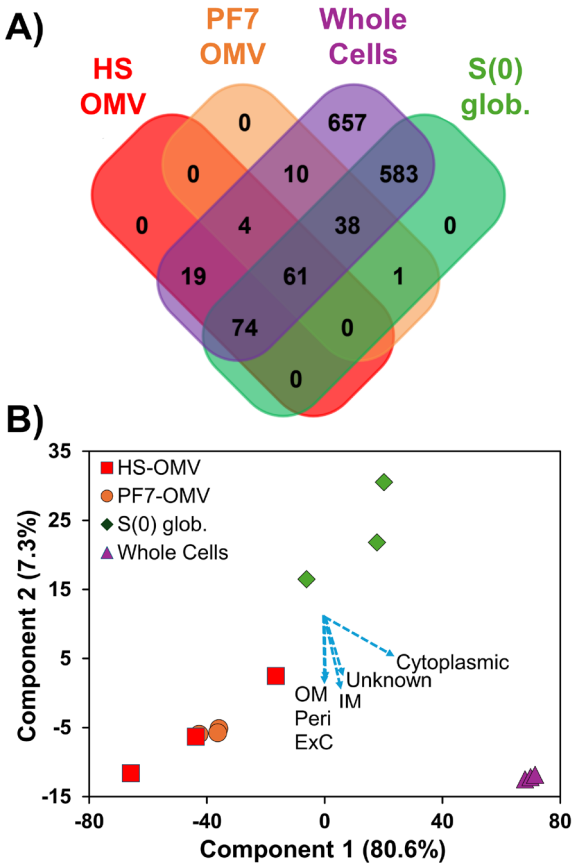

Figure 4. Comparative proteome analysis of *Cba. tepidum* whole cells, OMVs from cultures grown on sulfide (HS-OMV) or sulfide + thiosulfate (PF7-OMV), and biogenic sulfur globules (S(0) glob.). **A)** Venn diagram indicating the distribution of 1,447 proteins across sample group (n = 3 samples per group). **B)** Principal component analysis score plot of samples based on label free quantification. The first and the second principal components (PC) account for 80.6% and 7.3% of the variability in the data, respectively. Loadings for PC1 and PC2 are displayed (blue dashed arrows) for proteins grouped by PSORTb predicted localization: Cytoplasmic, Unknown, Inner Membrane (IM), Outer Membrane (OM), Periplasmic (Peri), and Extracellular (ExC).

799

800

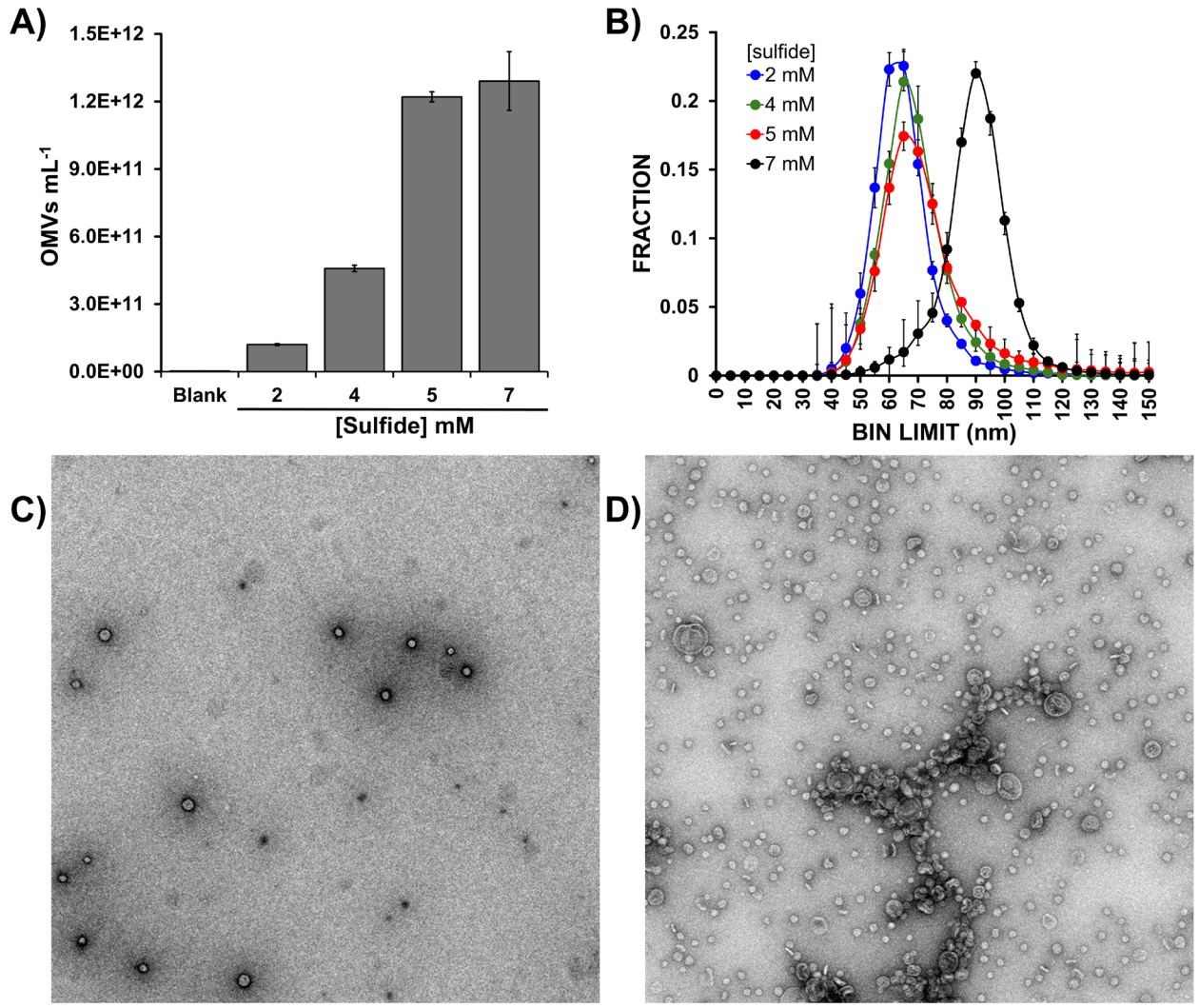

Figure 5. OMVs concentration and size vary with increased sulfide (HS) concentration. A) OMV concentrations measured after 14 h of growth with different concentrations of sulfide as the sole electron donor. B) MRSP-based size distribution of particles purified from the cultures in panel A (see Fig. S1A for purification details). C) and D) TEM analysis of OMVs purified from 4 mM and 7 mM sulfide cultures in panel A corresponding to the green and black traces in panel B.

801

802

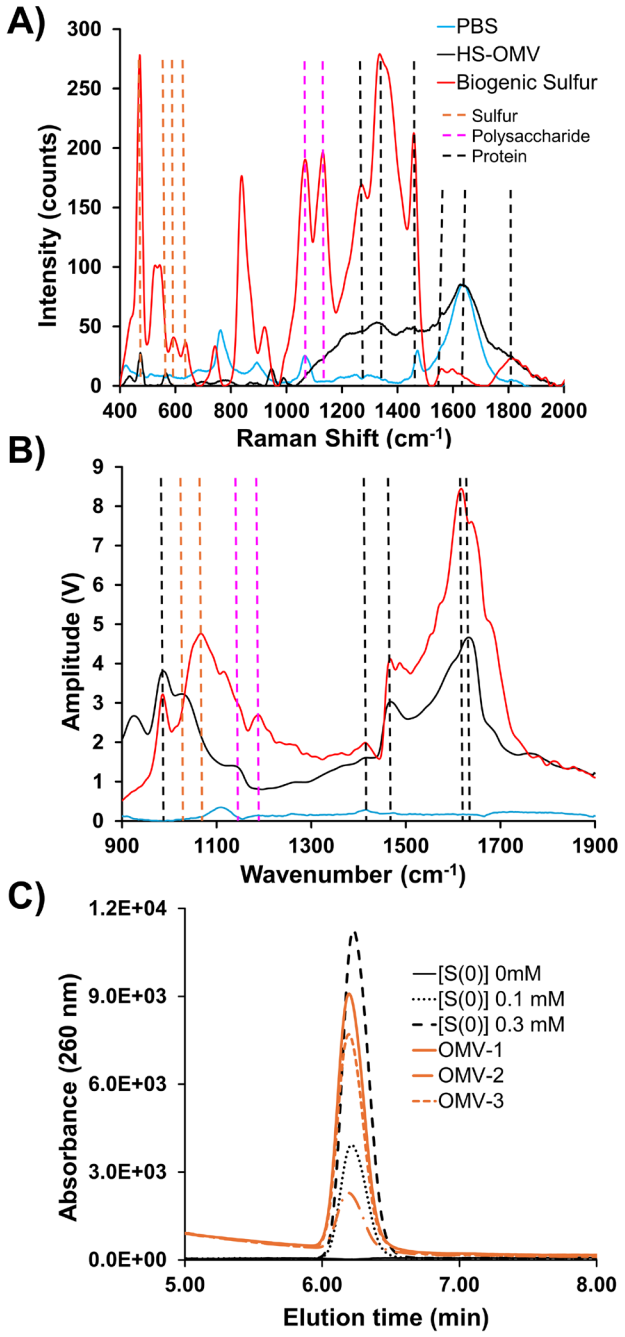

Figure 6. OMVs and S(0) share multiple characteristic. Characteristic Raman scattering **(A)** or IR absorption **(B)** spectra for purified OMVs (black), biogenic S(0) (red), and PBS (blue). Scattering (A) or absorption (B) wavenumbers are indicated by vertical dashed lines for sulfur (orange), polysaccharide (pink), and protein (black). **(C)** Chromatograms of elemental sulfur standards (0-0.3 mM S(0), black traces) and OMV's purified from three independent 7 mM sulfide *Cba. tepidum* cultures (orange traces). The standards indicate the peak from OMV samples co-migrates with authentic S(0) and the replicates are within the range of detection.

803

804

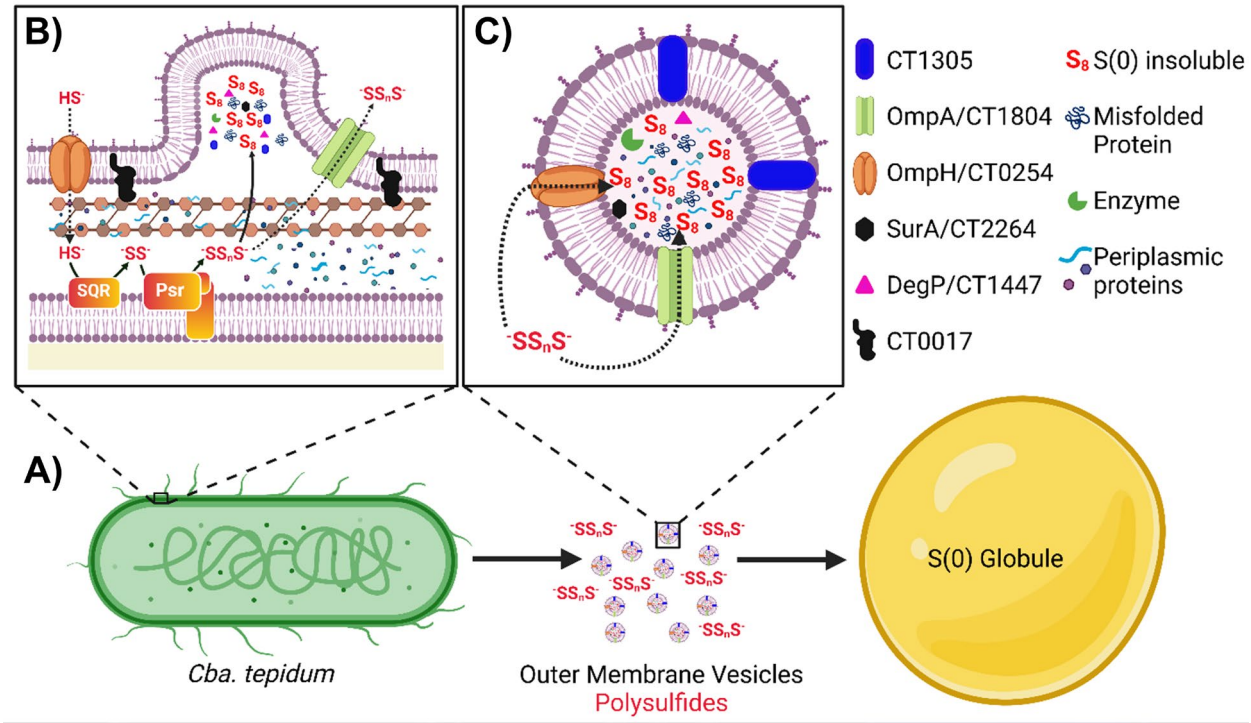

Figure 7. Summary of the proposed OMV S(0) transport mechanism. A) *Cba. tepidum* produces both OMVs and polysulfides during growth that contribute to the growth of extracellular S(0) globules. B) Enlarged view of the periplasm and OM with increased detail. Sulfide oxidation may induce unfolded protein stress that leads to OMV production. The dashed arrows for sulfide and polysulfide indicate possible routes to enter and exit either OMVs or S(0) globules. SQR = sulfide:quinone oxidoreductase (CT0117 and CT1087), Psr = putative polysulfide oxidoreductase complex (CT0496-CT0494). C) Enlarged view of a *Cba. tepidum* OMV with selected cargo molecules detected by proteomics analyses denoted at the right. Created in BioRender https://BioRender.com/bzod9yf

805

Table 1. OMV core proteins identified in ≥ 2 independent samples from each group (whole cells, S(0) globules, HS-OMV, and PF7-OMV) by label-free quantitative proteomics.

Locus Tag	Uniprot ID	PSORTb result	Description
CT0017	Q8KGF1	Unknown	Uncharacterized protein
CT0068	Q8KGA0	Unknown	Hemagglutinin-related protein
CT0073	Q8KG95	Unknown	Cytochrome c-555, membrane-bound
CT0075	Q8KG93	Periplasmic	Cytochrome c-555
CT0154	Q8KG16	Unknown	50S ribosomal protein L7/L12
CT0254	Q8KFR8	Unknown	Outer membrane protein OmpH
CT0351	Q9F722	InnerMembrane	Isocitrate dehydrogenase [NADP]
CT0529	Q8KFH5	Cytoplasmic	Co-chaperonin GroES
CT0530	Q8KF02	Cytoplasmic	Chaperonin GroEL
CT0636	Q8KEQ0	Periplasmic	Protein TolB homolog
CT0638	Q8KEP8	OuterMembrane	Peptidoglycan-associated protein
CT0640	Q8KEP6	Unknown	YfiO domain-containing protein
CT0643	Q8KEP3	Cytoplasmic	Chaperone protein DnaK
CT0865	Q8KE27	Cytoplasmic	Adenylylsulfate reductase, alpha subunit
CT0958	Q8KDT6	Extracellular	Uncharacterized protein
CT0984	Q8KDR1	OuterMembrane	Uncharacterized protein
CT1017	Q8KDM9	Unknown	Sulfur oxidation protein SoxY
CT1018	Q8KDM8	Unknown	Sulfur oxidation protein SoxZ
CT1054	Q8KDJ6	InnerMembrane	Carboxyl-terminal protease
CT1157	Q8KD97	Unknown	DUF4136 domain-containing protein
CT1201	Q8KD53	Unknown	DUF2934 domain-containing protein
CT1353	Q8KCR0	OuterMembrane	OmpA family protein
CT1447	Q8KCH4	Periplasmic	Serine protease, manually annotated as DegP
CT1745	Q8KBP0	Unknown	Uncharacterized protein/Transporter
CT1804	Q8KBI3	OuterMembrane	Porin_4 domain-containing protein
CT1900	Q8KB89	Unknown	Uncharacterized protein
CT1943	Q46367	Unknown	Chlorosome protein C
CT1953	Q8KB41	OuterMembrane	Ferric siderophore receptor, putative, TonB receptor family
CT1970	Q8KB28	Unknown	Heat shock protein, Hsp20 family
CT2054	Q46383	Unknown	Chlorosome envelope protein B
CT2144	Q8KAL2	OuterMembrane	Outer surface protein, putative
CT2191	Q8KAH0	Cytoplasmic	Elongation factor Tu
CT2264	Q8KAA2	Periplasmic	Peptidyl-prolyl cis-trans isomerase SurA
CT2270	Q8KA97	Unknown	Uncharacterized protein

806